Harnessing Higher-Dimensional Fluctuations in an Information Engine

Antonio Patrón Castro,* John Bechhoefer,† and David A. Sivak‡
Department of Physics, Simon Fraser University, Burnaby, British Columbia V5A 1S6, Canada

(Received 21 July 2025; accepted 22 December 2025; published 27 January 2026)

We study the optimal performance of an information engine consisting of an overdamped Brownian bead confined in a controllable, d-dimensional harmonic trap and additionally subjected to gravity. The trap's center is updated dynamically via a feedback protocol designed such that no external work is done by the trap on the bead while maximizing the extraction of gravitational potential energy and achieving directed motion. We show that performance improves when thermal fluctuations in directions perpendicular to gravity are harnessed. This improvement arises from feedback cooling of these transverse degrees of freedom, along which all heat is extracted. Strikingly, engines based on a single transverse degree of freedom already outperform engines based solely on vertical (z) measurements. This engine design modularizes the functions of harnessing fluctuations and storing free energy, drawing a close analogy to the Szilard engine.

DOI: 10.1103/xwjd-qxfg

Over a century ago, Maxwell proposed his famous thought experiment, suggesting that information about a system's microscopic dynamics could be used to extract useful energy without any work input—seemingly violating the second law of thermodynamics [1]. In the 1930s, Szilard refined this idea by introducing the first concrete model of what is now known as an *information engine* [2,3]: a cyclic device that exploits thermal fluctuations by applying feedback, thereby extracting heat from a thermal bath. Its operation is reconciled with the second law by Landauer's principle: Processing and erasing information about a system's dynamics has a minimum cost [4,5].

Recent advances in technology and stochastic thermodynamics [6–10] have enabled the experimental realization of modern information engines [11–20]. This capability has been used to test Landauer's principle and quantify the cost of information processing [21–27], cool nanoparticles to millikelvin temperatures [28–30], and confirm the limits of the second law [31–33]. Inspired by the ideas of Maxwell, Szilard, and Landauer, researchers have even constructed molecular-scale information engines, demonstrating that synthetic cyclic molecular machines can indeed leverage fluctuations to power their operation [34]. More recently, it has been suggested that many of the molecular motors operating within living cells (such as ATP synthase or kinesin) may also work as information engines, harnessing energy from the noisy cellular environment [35–39].

In previous work [40], Saha *et al.* designed and experimentally realized an information engine that, in addition to extracting energy from a thermal bath, stored such energy in a gravitational potential by raising a weight. Their engine consisted of a micron-scale bead in water, harmonically confined via optical tweezers [41,42]. The trap center was raised upon measuring a favorable "up" fluctuation of the bead (parallel to gravity). Subsequent studies explored performance for Bayesian inference of the bead's position under noisy measurements [43] and for nonequilibrium active noise [44–46].

To date, information engines have been essentially one-dimensional, exploiting fluctuations along a single degree of freedom. Can harnessing fluctuations along additional degrees of freedom further improve performance? In this Letter, we generalize a theoretical study of the experimental engine of [47] to d dimensions and find striking increases in the rate of energy extraction and related measures of performance. We show that the performance enhancement results from feedback cooling of thermal fluctuations along the transverse degrees of freedom, thereby extracting *all* available heat, since all such fluctuations are favorable. We demonstrate that feedback on the transverse degrees of freedom alone can produce high output power, by analyzing an engine variant in which we do not measure the vertical z component. This engine design separates the essential functions of harnessing fluctuations and storing free energy, capturing a core feature of the original Szilard engine. These results highlight the potential of higher-dimensional fluctuations as a valuable resource in the design of information engines and underscore the importance of choosing which degrees of freedom to measure and their impact in overall engine performance.

Multidimensional information engine—Consider an optically trapped bead in d spatial dimensions, whose dynamics are governed by the overdamped Langevin equation

*Contact author: apatronc@sfu.ca
†Contact author: johnb@sfu.ca
‡Contact author: dsivak@sfu.ca

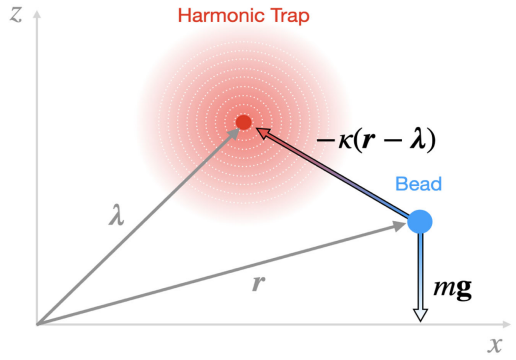

FIG. 1. Schematic for $d = 2$: a Brownian bead (blue dot) at position $\boldsymbol{r} = (x, z)$ experiences the gravitational force in the z direction and the action of a confining optical trap (red dot and area) centered at $\boldsymbol{\lambda}$.

$$\gamma\dot{\boldsymbol{r}}'(t') = -\kappa[\boldsymbol{r}'(t') - \boldsymbol{\lambda}'(t')] - m\boldsymbol{g} + \sqrt{2k_{\mathrm{B}}T\gamma}\boldsymbol{\xi}(t'), \quad (1)$$

for bead position $\boldsymbol{r}'(t')$ at time t', isotropic harmonic trap center $\boldsymbol{\lambda}'(t')$, trap stiffness κ, bead mass m relative to the surrounding fluid, gravitational acceleration $\boldsymbol{g}$, friction coefficient γ, Boltzmann constant k_{B}, and thermal-bath temperature T. $\boldsymbol{\xi}(t')$ is a vector of Gaussian white-noise fluctuations of zero mean and correlations

$$\left\langle \xi^{(i)}(t_1')\xi^{(j)}(t_2') \right\rangle = \delta_{ij}\delta(t_1' - t_2'), \quad \forall\ i, j = 1, \ldots, d. \quad (2)$$

We nondimensionalize the problem by scaling lengths with the equilibrium standard deviation $\sigma_{\mathrm{eq}} \equiv \sqrt{k_{\mathrm{B}}T/\kappa}$ of the bead's position and time with the relaxation time $\tau_{\mathrm{r}} \equiv \kappa/\gamma$. This yields the dimensionless variables $t \equiv t'/\tau_{\mathrm{r}}$, $\boldsymbol{r}(t) \equiv \boldsymbol{r}'(t')/\sigma_{\mathrm{eq}}$, and $\boldsymbol{\lambda}(t) \equiv \boldsymbol{\lambda}'(t')/\sigma_{\mathrm{eq}}$ and the dimensionless overdamped Langevin equation

$$\dot{\boldsymbol{r}}(t) = -[\boldsymbol{r}(t) - \boldsymbol{\lambda}(t)] - \boldsymbol{\delta}_{\mathrm{g}} + \sqrt{2}\boldsymbol{\xi}(t), \quad (3)$$

where $\boldsymbol{\delta}_{\mathrm{g}} \equiv m\boldsymbol{g}/\kappa\sigma_{\mathrm{eq}}$ is a dimensionless vector quantifying the gravitational force relative to the amplitude of thermal fluctuations. Figure 1 illustrates the system for $d = 2$.

The total, time-dependent potential for the bead results from the combination of the optical trap and the gravitational force:

$$V(\boldsymbol{r}, \boldsymbol{\lambda}(t)) = \frac{1}{2}|\boldsymbol{r} - \boldsymbol{\lambda}(t)|^2 + \boldsymbol{r}^{\top}\boldsymbol{\delta}_{\mathrm{g}}. \quad (4)$$

The bead's position is measured at discrete time intervals of duration t_{s}, and the feedback on the trap position is applied immediately. Integrating Eq. (1) over one time step provides the discrete-time dynamics [47,48]:

$$\boldsymbol{r}_{n+1} = e^{-t_{\mathrm{s}}}\boldsymbol{r}_n + (1 - e^{-t_{\mathrm{s}}})(\boldsymbol{\lambda}_{n^+} - \boldsymbol{\delta}_{\mathrm{g}}) + \sqrt{1 - e^{-2t_{\mathrm{s}}}}\boldsymbol{\nu}_n, \quad (5)$$

for time step number n and vector $\boldsymbol{\nu}_n$ of Gaussian random variables with zero mean and correlations

$$\left\langle \nu_n^{(i)}\nu_{n'}^{(j)} \right\rangle = \delta_{ij}\delta_{nn'}, \quad \forall\ i, j = 1, \ldots, d. \quad (6)$$

The subscript n^+ indicates that $\boldsymbol{\lambda}$ is updated *after* measuring $\boldsymbol{r}$. To simplify analysis and aid physical interpretation, we choose an orthogonal coordinate system such that $\boldsymbol{r} = (x^{(1)}, x^{(2)}, \ldots, x^{(d-1)}, z)$ and $\boldsymbol{\lambda} = (\lambda^{(1)}, \lambda^{(2)}, \ldots, \lambda^{(d-1)}, \lambda^{(z)})$, for z the degree of freedom parallel to the gravitational force. With this choice of coordinates, z is influenced by both the gravitational force and the harmonic trap, whereas the remaining degrees of freedom are driven only by the harmonic trap. Throughout, $\{x^{(i)}\}$ and $\{\lambda^{(i)}\}$ are the transverse components of the bead and trap center, respectively, which live on the orthogonal $(d-1)$-dimensional space $\mathbb{R}_{d-1}$.

After updating bead position $\boldsymbol{r}_n$ to $\boldsymbol{r}_{n+1}$, the trap position $\boldsymbol{\lambda}$ is updated according to a feedback algorithm, chosen (following [47]) to optimize two performance metrics. The first metric is the net output power

$$P_{\mathrm{net}} = f_{\mathrm{s}}(\langle \Delta F \rangle - \langle W \rangle), \quad (7)$$

for sampling frequency $f_{\mathrm{s}} \equiv 1/t_{\mathrm{s}}$, and per-measurement average stored equilibrium free energy $\langle \Delta F \rangle$ and work $\langle W \rangle$ done on the bead. The averages are taken over the system probability distribution at steady state. Here, work is the instantaneous change in the total potential when the trap center $\boldsymbol{\lambda}$ is updated:

$$W_{n+1} \equiv V(\boldsymbol{r}_{n+1}, \boldsymbol{\lambda}_{n^+ + 1}) - V(\boldsymbol{r}_{n+1}, \boldsymbol{\lambda}_{n^+}) \quad (8a)$$

$$= \frac{1}{2}|\boldsymbol{r}_{n+1} - \boldsymbol{\lambda}_{n^+ + 1}|^2 - \frac{1}{2}|\boldsymbol{r}_{n+1} - \boldsymbol{\lambda}_{n^+}|^2. \quad (8b)$$

By convention, work is positive if energy flows into the system from the harmonic trap. Similarly, the average stored equilibrium free energy is

$$\langle \Delta F \rangle = \delta_{\mathrm{g}}\left\langle \lambda_{n^+ + 1}^{(z)} - \lambda_{n^+}^{(z)} \right\rangle. \quad (9)$$

From the first law of thermodynamics for the bead at steady state, the net output power P_{net} equals the rate of heat extraction from the environment [40]. This follows from the assumption that no energy is exchanged between the bead and the controller, such that all stored energy is in the form of gravitational free energy. We focus on pure information engines, where exactly no work is done by each trap movement ($W_{n+1} = 0$). As a result, these engines store useful free energy by exploiting thermal fluctuations alone: Heat is continuously extracted from the thermal bath without any external work input.

The feedback algorithm is then chosen such that (i) the harmonic trap does no work on the system and (ii) the

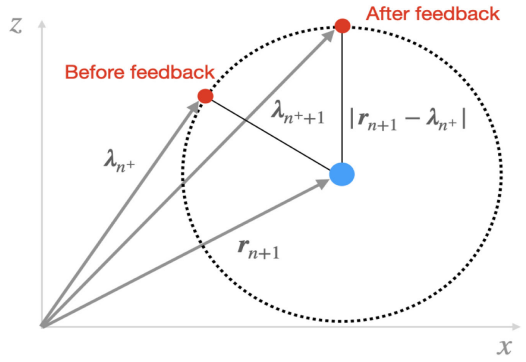

FIG. 2. Schematic of the zero-work condition and the optimal feedback rule maximizing free-energy storage for $d = 2$. The dashed circle shows possible updated positions $\boldsymbol{\lambda}_{n^+\!+1}$ for the trap center, given $\boldsymbol{r}_{n+1}$ and $\boldsymbol{\lambda}_{n^+}$, for which no work is exerted on the bead. The updated trap center lies at the top of a hypersphere centered at $\boldsymbol{r}_{n+1}$ with radius $|\boldsymbol{r}_{n+1} - \boldsymbol{\lambda}_{n^+}|$.

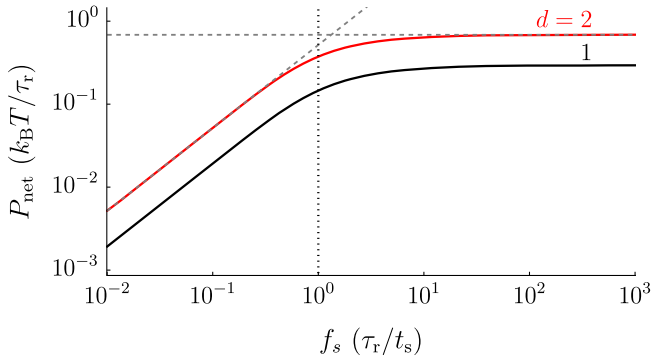

FIG. 3. Information-engine output power $P_{\rm net}$ as a function of sampling frequency $f_{\rm s}$, for $d = 2$ (red) and $d = 1$ (black). Solid curves: semianalytic steady-state calculations (Sec. IV in Supplementary Material [49] and [47]). Dashed gray lines: analytic results in the low-sampling-frequency limit (Sec. III in Supplementary Material [49]) and the high-sampling-frequency limit (13). The dotted vertical line indicates $f_{\rm s} = 1$. We set $\delta_{\rm g} = 0.8$, the value that approximately maximizes the output power for $d = 1$ [47].

stored free energy is maximized (Sec. I in Supplementary Material [49]), giving

$$\boldsymbol{\lambda}_{n^+\!+1} = \boldsymbol{r}_{n+1} + |\boldsymbol{r}_{n+1} - \boldsymbol{\lambda}_{n^+}|\hat{\boldsymbol{z}}, \tag{10}$$

for unit vector $\hat{\boldsymbol{z}}$. The zero-work condition $W_{n+1} = 0$ constrains $\boldsymbol{\lambda}_{n^+\!+1}$ to a hypersphere centered at $\boldsymbol{r}_{n+1}$ with radius $|\boldsymbol{r}_{n+1} - \boldsymbol{\lambda}_{n^+}|$, and the free-energy maximization further restricts $\boldsymbol{\lambda}_{n^+\!+1}$ to the top of this hypersphere. Thus, a down fluctuation in z does not prevent harnessing a simultaneous lateral fluctuation to lift the equilibrium trap position. Figure 2 illustrates both the zero-work condition and the optimal feedback rule (10) for a $d = 2$ pure information engine.

Resolving the vertical and transverse components gives

$$\lambda^{(z)}_{n^+\!+1} = z_{n+1} + \sqrt{\left(z_{n+1} - \lambda^{(z)}_{n^+}\right)^2 + \sum_{j=1}^{d-1}\left(\Delta x^{(j)}_{n+1}\right)^2}, \tag{11a}$$

$$\lambda^{(i)}_{n^+\!+1} = x^{(i)}_{n+1}, \quad i = 1, 2, \ldots, d-1, \tag{11b}$$

with bead update $\Delta x^{(j)}_{n+1} \equiv x^{(j)}_{n+1} - x^{(j)}_{n} = x^{(j)}_{n+1} - \lambda^{(j)}_{n^+}$ equaling the bead position relative to the trap center. The trap's z component stores gravitational free energy, while the transverse components track the bead's transverse position (so transverse fluctuations are isotropic), effectively enacting a *feedback cooling* protocol that maximizes heat extraction in Brownian engines [51]. Any gain in potential energy due to transverse fluctuations is transferred to stored free energy during the subsequent trap update.

The second performance metric is the long-time average z velocity $\langle v_z \rangle$, which for a pure information engine is proportional to the output power [47]:

$$P_{\rm net} = \delta_{\rm g}\langle v_z \rangle. \tag{12}$$

This metric is directly accessible in experiments and quantifies the information engine's ability to generate directed motion against the load from an external force.

Optimal performance—We first examine the dependence of performance on the sampling frequency $f_{\rm s}$ for fixed $\delta_{\rm g} = 0.8$, chosen because it was previously shown to (approximately) maximize the output power for $d = 1$ [47]. In Fig. 3, we compare the performance of a $d = 2$ engine with the previously characterized $d = 1$ engine. The two engines exhibit similar behavior. At high sampling frequencies, the output power and heat extraction saturate. In this regime, the trap-center dynamics approximately follow a Langevin-like equation, producing maximum output power

$$P^{\rm HF}_{\rm net}(\delta_{\rm g}) = (d-1)\delta_{\rm g}\frac{\mathcal{Z}_{d-1}(\delta_{\rm g})}{\mathcal{Z}_d(\delta_{\rm g})}, \tag{13}$$

for partition function

$$\mathcal{Z}_d(\delta_{\rm g}) \equiv \int_0^\infty \mathrm{d}L\, L^{d-1} e^{-L^2/2 + \delta_{\rm g} L}, \tag{14}$$

expressible in terms of hypergeometric functions (Sec. II in Supplementary Material [49]). Equation (13) holds even for $d \to 1$, recovering the $d = 1$ expression for the output power from [47].

At low sampling frequencies $f_{\rm s}$, ratchet events occur with frequency proportional to $f_{\rm s}$, as the bead's position equilibrates between measurements. Consequently, the average stored equilibrium free energy in Eq. (9) reaches a constant value, so the output power is linear in $f_{\rm s}$ (Sec. III in Supplementary Material [49]). The transition between the two limiting behaviors takes place around $f_{\rm s} = 1$,

where the sampling time $t_s \approx \tau_r$. Despite the similar trends, the $d = 2$ engine nearly doubles the output power attained by its $d = 1$ counterpart.

The comparison between the performances of the $d = 2$ and $d = 1$ information engines already suggests that fluctuations in degrees of freedom perpendicular to gravity can be exploited to enhance heat extraction. In Sec. V in Supplementary Material [49], we investigate whether it is better to exploit all such transverse fluctuations or to wait for rare large ones which give a higher increase in stored free energy. To address this, we introduce a modified feedback rule, in which the trap center is updated only when, at the time of measurement, the bead lies outside a cylinder of radius R. The threshold R setting the minimum fluctuation size is centered on the trap position and aligned with the z axis. We show that the output power decreases monotonically with R, maximized at $R = 0$. Therefore, the optimal strategy exploits *all* available transverse fluctuations, regardless of their size.

Having shown that continuous sampling and continuous ratcheting optimize performance, we study the dependence of the output power and the vertical velocity on the dimensionless force δ_g. For $d = 1$, the optimal output power at $\delta_g^* \approx 0.8$ arises from two competing factors: On the one hand, as we increase δ_g from 0, the potential energy to extract increases. On the other hand, the magnitude of the opposing force also increases, making significant up fluctuations unlikely. This competition leads to maximum output power at an intermediate δ_g.

Surprisingly, the nonmonotonic dependence on δ_g is not seen in higher dimensions. Figure 4 shows the output power and the vertical velocity as functions of the opposing gravitational force δ_g, for different dimensions. The output power is maximized in the $\delta_g \to \infty$ limit for $d > 1$, asymptoting to $d - 1$, which implies that the velocity decays to zero algebraically as δ_g increases ($\sim 1/\delta_g$), in contrast to the exponential $\exp\{-\delta_g^2/2\}$ decay in one dimension [47]. Approximating the partition function (14) for $\delta_g \to \infty$ using Laplace's method [50] gives $P_{\rm net}^{\rm HF}(\delta_g) \sim d - 1$.

The fact that the output power asymptotically approaches $d - 1$ (in dimensionless units) for large δ_g has striking implications. The output power is bounded above by the value attained under feedback cooling—where the trap follows the bead after each measurement, thereby extracting all the thermal fluctuations in potential energy. For feedback cooling, the power extracted by each independent degree of freedom is 1 [51], and, hence, the overall power for $d - 1$ feedback-cooled degrees of freedom equals $d - 1$. Our findings suggest that our information engine extracts the maximum possible power from the $d - 1$ transverse degrees of freedom, while the z component contributes no significant heat extraction, since in this limit useful up fluctuations against gravity become very unlikely. This interpretation is supported by the explicit componentwise form of the feedback rule in Eq. (10): The z degree of freedom adjusts to satisfy the zero-work condition, whereas the transverse degrees of freedom follow the feedback-cooling protocol, thereby maximizing heat extraction along those directions.

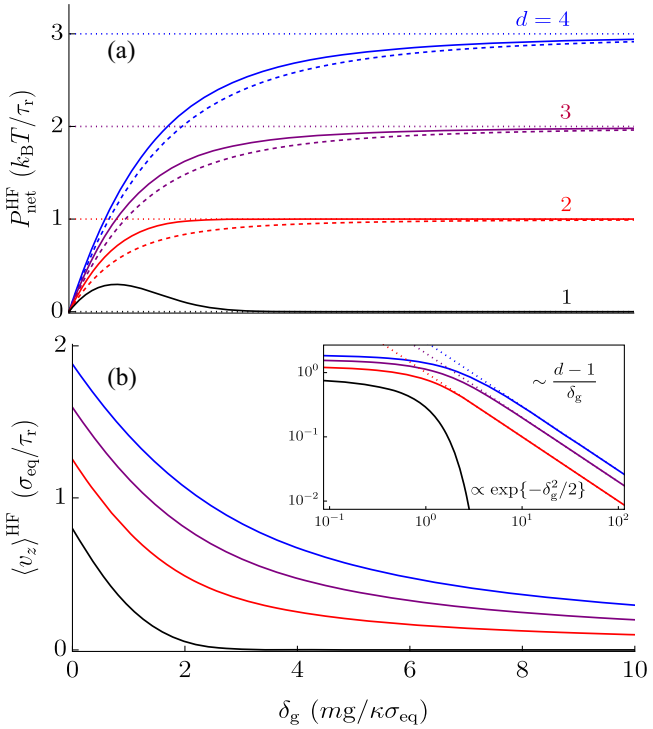

FIG. 4. Output power (a) and vertical velocity (b) as functions of the scaled gravitational force δ_g, in the high-sampling frequency limit, for different dimensions. Solid curves: analytic results (13) (Sec. II in Supplementary Material [49]). Dashed curves: partial information engine from Eq. (16). Dotted lines: asymptotic limit $d - 1$ for $\delta_g \to \infty$. Inset in (b): log-log plot highlighting the algebraic decay for large δ_g, whose analytic form is represented by dotted lines.

Ignoring vertical fluctuations—In the previous section, we showed that, in the $\delta_g \gg 1$ limit, the output power of a d-dimensional information engine is equal to feedback cooling of the $d - 1$ degrees of freedom perpendicular to the gravitational force. The z-component fluctuations, parallel to gravity, do not contribute to the engine's performance. This observation raises a natural question: Is it necessary to measure the z component in this regime, or is it sufficient to measure only the transverse components? To address this, we consider a *partial* information engine, in which the feedback rule depends only on measurements of the $d - 1$ transverse degrees of freedom, ignoring the z component of the bead's position. For clarity, we refer to the previously studied system as the *complete* information engine.

Since we do not measure the z component, the zero-work condition $W_{n+1} = 0$ cannot be rigorously fulfilled at each time step. Instead, we design a feedback rule for a pure information engine such that the average work $\langle W_{n+1} \rangle$ is zero. This dictates a feedback rule for $\lambda_{n^+ +1}^{(z)}$ of the form

$$\lambda^{(z)}_{n^+_{+1}} = \lambda^{(z)}_{n^+} + \left\langle z_{n+1} - \lambda^{(z)}_{n^+} \right\rangle + \sqrt{\left\langle z_{n+1} - \lambda^{(z)}_{n^+} \right\rangle^2 + \sum_{j=1}^{d-1} \left(\Delta x^{(j)}_{n+1} \right)^2}, \quad (15)$$

with $\lambda^{(i)}_{n^+_{+1}}$ following Eq. (11b). The averages are taken over the steady-state distribution for the relative displacements $z_{n+1} - \lambda^{(z)}_{n^+}$. In Sec. VI in Supplementary Material [49], we derive an analytical expression for the output power in the limit of high sampling frequencies:

$$P^{\mathrm{HF}}_{\mathrm{net}}(\delta_{\mathrm{g}}) = \frac{2(d-1)}{1 + \sqrt{1 + 4(d-1)/\delta^2_{\mathrm{g}}}}. \quad (16)$$

Figure 4(a) shows that the complete and partial information engines attain the same output power for $\delta_{\mathrm{g}} \to \infty$, consistent with our previous result that, in that limit, the z fluctuations do not contribute to free-energy extraction. For intermediate δ_{g}, Fig. 4(a) shows that measuring z has some small advantage, permitting the harnessing of some z fluctuations. But even in the simplest scenario, measuring a single transverse degree of freedom (x for the $d = 2$ partial information engine) increases output power remarkably compared to measuring only z as in the original $d = 1$ engine.

Conclusions—We have studied the theoretical performance of an information engine that harnesses thermal fluctuations in a d-dimensional overdamped system to achieve directed motion against gravity, thus converting heat from the thermal bath into stored gravitational potential energy. Systematically optimizing the engine's output power and velocity, we have shown that our $d > 1$-dimensional engine significantly outperforms the previously studied $d = 1$ engine [41,47]. The increase in stored free energy per dimension can be viewed as a decrease in the available phase-space volume following the symmetry-breaking event of measuring the bead's position [52].

The mechanism behind this enhancement is intimately related to feedback cooling: The $d - 1$ transverse degrees of freedom each extract $k_{\mathrm{B}}T/\tau_{\mathrm{r}}$—the maximum amount of heat available per dimension—whereas heat extraction in the z component is limited by gravity. Indeed, in the $\delta_{\mathrm{g}} \to \infty$ limit, the output power saturates to $d - 1$ (in units of $k_{\mathrm{B}}T/\tau_{\mathrm{r}}$), implying that operation is sustained only by the transverse degrees of freedom. This is further confirmed by the partial information engine considered in Eq. (15): Even without measurements of the bead's z component, the engine still achieves the same limiting performance for large δ_{g}, with minor deviations from the complete engine for intermediate values of δ_{g}. These results suggest that choosing which degrees of freedom to measure may play a dominant role in the overall engine performance. This is similar to the problem of identifying suitable reaction coordinates for efficient enhanced sampling of free-energy landscapes in complex molecular systems [53,54]. Thus, our Letter provides a design principle that could guide the next-generation of nanoscale energy-harvesting devices [55–57].

In this Letter, we have focused on maximizing engine performance, without considering the information costs that result from nearly continuous measurement of the bead's position. An important direction for future work involves the experimental realization of the $d = 2$ and $d = 3$ engines based on nanoscale Brownian objects confined in optical traps, which are straightforward extensions of existing $d = 1$ information engines [47,51]. Further research could also consider the measurement and information-processing costs of the measuring devices and uncertainties in position and time measurements. A full accounting of all entropy production requires including these information-processing costs [11,18,58–60]. The high-sampling-frequency limit (where we measure much faster than the system's characteristic dynamical timescales) pays large information costs for diminishing benefit. The partial information engine from Eq. (15) is thus more efficient, gathering and processing less information to attain similar heat extraction.

More broadly, it would be interesting to explore the role of higher-dimensional fluctuations in different information engines involving more complex physical mechanisms. Promising directions include underdamped dynamics [26,61–65], where applying feedback to velocity measurements improves engine control [66,67]; multicomponent molecular motors, where energy and information flow between the system's different components to transduce free energy [35–39]; and active noise, where the nonequilibrium bath serves as an additional source of fluctuations [45,68–72], giving information engines a potential advantage over conventional heat engines.

Acknowledgments—We thank Matthew Leighton (Yale Physics) and Johan du Buisson (Tubingen Theoretical Physics) for fruitful feedback on the manuscript. This work was supported by a Natural Sciences and Engineering Research Council of Canada (NSERC) Discovery Grant (J. B.), an NSERC Discovery Grant and Discovery Accelerator Supplement RGPIN-2020-04950 (D. A. S.), an NSERC Alliance International Collaboration Grant No. ALLRP-2023-585940 (D. A. S.), and a Tier-II Canada Research Chair CRC-2020-00098 (D. A. S.). This research was enabled in part by support provided by BC DRI Group and the Digital Research Alliance of Canada.

Data availability—The data that support the findings of this article are openly available [73].

[1] C. G. Knott, *Life and Scientific Work of Peter Guthrie Tait* (Cambridge University Press, London, 1911), https://archive.org/details/lifescientificwo00knotuoft.

[2] L. Szilard, Über die entropieverminderung in einem thermodynamischen system bei eingriffen intelligenter wesen, Z. Phys. **53**, 840 (1929).

[3] L. Szilard, On the decrease of entropy in a thermodynamic system by the intervention of intelligent beings, Behav. Sci. **9**, 301 (1964).
[4] R. Landauer, Irreversibility and heat generation in the computing process, IBM J. Res. Dev. **5**, 183 (1961).
[5] C. H. Bennett, The thermodynamics of computation—A review, Int. J. Theor. Phys. **21**, 905 (1982).
[6] K. Sekimoto, Kinetic characterization of heat bath and the energetics of thermal ratchet models, J. Phys. Soc. Jpn. **66**, 1234 (1997).
[7] K. Sekimoto, *Stochastic Energetics*, Lecture Notes in Physics, Vol. 799 (Springer, New York, 2010), 10.1007/978-3-642-05411-2.
[8] U. Seifert, Stochastic thermodynamics, fluctuation theorems and molecular machines, Rep. Prog. Phys. **75**, 126001 (2012).
[9] C. V. den Broeck and M. Esposito, Ensemble and trajectory thermodynamics: A brief introduction, Physica (Amsterdam) **418A**, 6 (2015).
[10] U. Seifert, *Stochastic Thermodynamics* (Cambridge University Press, Cambridge, England, 2025), https://www.cambridge.org/core/books/stochastic-thermodynamics/1766FFBF10FCC7A75DAA89C6E09ED0AB.
[11] S. Toyabe, T. Sagawa, M. Ueda, E. Muneyuki, and M. Sano, Experimental demonstration of information-to-energy conversion and validation of the generalized Jarzynski equality, Nat. Phys. **6**, 988 (2010).
[12] P. A. Camati, J. P. S. Peterson, T. B. Batalhao, K. Micadei, A. M. Souza, R. E. Sarthour, I. S. Oliveira, and R. M. Serra, Experimental rectification of entropy production by Maxwell's demon in a quantum system, Phys. Rev. Lett. **117**, 240502 (2016).
[13] J. V. Koski, A. Kutvonen, I. M. Khaymovich, T. Ala-Nissila, and J. P. Pekola, On-chip Maxwell's demon as an information-powered refrigerator, Phys. Rev. Lett. **115**, 260602 (2015).
[14] N. Cottet, S. Jezouin, L. Bretheau, P. Campagne-Ibarcq, Q. Ficheux, J. Anders, A. Auffèves, R. Azouit, P. Rouchon, and B. Huard, Observing a quantum Maxwell demon at work, Proc. Natl. Acad. Sci. U.S.A. **114**, 7561 (2017).
[15] Y. Masuyama, K. Funo, Y. Murashita, A. Noguchi, S. Kono, Y. Tabuchi, R. Yamazaki, M. Ueda, and Y. Nakamura, Information-to-work conversion by Maxwell's demon in a superconducting circuit quantum electrodynamical system, Nat. Commun. **9**, 1291 (2018).
[16] J. V. Koski, V. F. Maisi, J. P. Pekola, and D. V. Averin, Experimental realization of a Szilard engine with a single electron, Proc. Natl. Acad. Sci. U.S.A. **111**, 13786 (2014).
[17] K. Chida, S. Desai, K. Nishiguchi, and A. Fujiwara, Power generator driven by Maxwell's demon, Nat. Commun. **8**, 15310 (2017).
[18] T. Admon, S. Rahav, and Y. Roichman, Experimental realization of an information machine with tunable temporal correlations, Phys. Rev. Lett. **121**, 180601 (2018).
[19] R. Goerlich, L. Hoek, O. Chor, S. Rahav, and Y. Roichman, Experimental realizations of information engines: Beyond proof of concept, Europhys. Lett. **149**, 61001 (2025).
[20] M. Baldovin, I. Ben Yedder, C. A. Plata, D. Raynal, L. Rondin, E. Trizac, and A. Prados, Optimal control of levitated nanoparticles through finite-stiffness confinement, Phys. Rev. Lett. **135**, 097102 (2025).
[21] A. Bérut, A. Arakelyan, A. Petrosyan, S. Ciliberto, R. Dillenschneider, and E. Lutz, Experimental verification of Landauer's principle linking information and thermodynamics, Nature (London) **483**, 187 (2012).
[22] Y. Jun, M. Gavrilov, and J. Bechhoefer, High-precision test of Landauer's principle in a feedback trap, Phys. Rev. Lett. **113**, 190601 (2014).
[23] J. V. Koski, V. F. Maisi, T. Sagawa, and J. P. Pekola, Experimental observation of the role of mutual information in the nonequilibrium dynamics of a Maxwell demon, Phys. Rev. Lett. **113**, 030601 (2014).
[24] J. Hong, B. Lambson, D. Scott, and J. Bokor, Experimental test of Landauer's principle in single-bit operations on nanomagnetic memory bits, Sci. Adv. **2**, e1501492 (2016).
[25] S. Ciliberto, Landauer's bound and Maxwell's demon, in *Information Theory: Poincaré Seminar 2018*, edited by B. Duplantier and V. Rivasseau (Springer International Publishing, Cham, 2021), pp. 87–112, 10.1007/978-3-030-81480-9_3.
[26] S. Dago, J. Pereda, N. Barros, S. Ciliberto, and L. Bellon, Information and thermodynamics: Fast and precise approach to Landauer's bound in an underdamped micromechanical oscillator, Phys. Rev. Lett. **126**, 170601 (2021).
[27] A. Archambault, C. Crauste-Thibierge, A. Imparato, C. Jarzynski, S. Ciliberto, and L. Bellon, Information engine fueled by first-passage times, Phys. Rev. Lett. **135**, 147101 (2025).
[28] T. Li, S. Kheifets, and M. G. Raizen, Millikelvin cooling of an optically trapped microsphere in vacuum, Nat. Phys. **7**, 527 (2011).
[29] J. Gieseler, B. Deutsch, R. Quidant, and L. Novotny, Subkelvin parametric feedback cooling of a laser-trapped nanoparticle, Phys. Rev. Lett. **109**, 103603 (2012).
[30] F. Tebbenjohanns, M. Frimmer, A. Militaru, V. Jain, and L. Novotny, Cold damping of an optically levitated nanoparticle to microkelvin temperatures, Phys. Rev. Lett. **122**, 223601 (2019).
[31] N. Barros, S. Ciliberto, and L. Bellon, Probabilistic work extraction on a classical oscillator beyond the second law, Phys. Rev. Lett. **133**, 057101 (2024).
[32] G. Paneru, S. Dutta, T. Tlusty, and H. K. Pak, Reaching and violating thermodynamic uncertainty bounds in information engines, Phys. Rev. E **102**, 032126 (2020).
[33] J. Klinger and G. M. Rotskoff, Universal energy-speed-accuracy trade-offs in driven nonequilibrium systems, Phys. Rev. E **111**, 014114 (2025).
[34] V. Serreli, C. Lee, E. R. Kay, and D. A. Leigh, A molecular information ratchet, Nature (London) **445**, 523 (2007).
[35] M. P. Leighton and D. A. Sivak, Inferring subsystem efficiencies in bipartite molecular machines, Phys. Rev. Lett. **130**, 178401 (2023).
[36] M. P. Leighton, J. Ehrich, and D. A. Sivak, Information arbitrage in bipartite heat engines, Phys. Rev. X **14**, 041038 (2024).
[37] M. P. Leighton and D. A. Sivak, Flow of energy and information in molecular machines, Annu. Rev. Phys. Chem. **76**, 379 (2025).

[38] T. Tsuruyama, Rna polymerase is a unique Maxwell's demon that converts its transcribing genetic information to free energy for its movement, Eur. Phys. J. Plus **138**, 1 (2023).
[39] J. M. R. Parrondo, J. M. Horowitz, and T. Sagawa, Thermodynamics of information, Nat. Phys. **11**, 131 (2015).
[40] J. du Buisson, D. A. Sivak, and J. Bechhoefer, Performance limits of information engines, Adv. Phys. X **9**, 2352112 (2024).
[41] Joseph N. E. Lucero, J. Ehrich, J. Bechhoefer, and D. A. Sivak, Maximal fluctuation exploitation in Gaussian information engines, Phys. Rev. E **104**, 044122 (2021).
[42] T. K. Saha and J. Bechhoefer, Optical trapping and optical micromanipulation, Proc. SPIE Int. Soc. Opt. Eng. **11798**, 53 (2021).
[43] T. K. Saha, Joseph N. E. Lucero, J. Ehrich, D. A. Sivak, and J. Bechhoefer, Bayesian information engine that optimally exploits noisy measurements, Phys. Rev. Lett. **129**, 130601 (2022).
[44] T. K. Saha, J. Ehrich, M. Gavrilov, S. Still, D. A. Sivak, and J. Bechhoefer, Information engine in a nonequilibrium bath, Phys. Rev. Lett. **131**, 057101 (2023).
[45] G. Paneru, S. Dutta, and H. K. Pak, Colossal power extraction from active cyclic Brownian information engines, J. Phys. Chem. Lett. **13**, 6912 (2022).
[46] G. Paneru, D. Y. Lee, J.-M. Park, J. T. Park, J. D. Noh, and H. K. Pak, Optimal tuning of a Brownian information engine operating in a nonequilibrium steady state, Phys. Rev. E **98**, 052119 (2018).
[47] T. K. Saha, J. N. E. Lucero, J. Ehrich, D. A. Sivak, and J. Bechhoefer, Maximizing power and velocity of an information engine, Proc. Natl. Acad. Sci. U.S.A. **118**, e2023356118 (2021).
[48] P. E. Kloeden and E. Platen, *Numerical Solution of Stochastic Differential Equations* (Springer, Berlin, Heidelberg, 1992), 10.1007/978-3-662-12616-5.
[49] See Supplemental Material at http://link.aps.org/supplemental/10.1103/xwjd-qxfg for details of the derivations and numerical methods, which includes Refs. [47,48,50].
[50] C. M. Bender and S. A. Orszag, *Advanced Mathematical Methods for Scientists and Engineers* (McGraw-Hill, New York, 1978), 10.1007/978-1-4757-3069-2.
[51] D. Y. Lee, J. Um, G. Paneru, and H. K. Pak, An experimentally-achieved information-driven Brownian motor shows maximum power at the relaxation time, Sci. Rep. **8**, 12121 (2018).
[52] E. Roldán, I. A. Martínez, J. M. R. Parrondo, and D. Petrov, Universal features in the energetics of symmetry breaking, Nat. Phys. **10**, 457 (2014).
[53] A. Ma and H. Li, Reaction coordinates are optimal channels of energy flow, Annu. Rev. Phys. Chem. **76**, 153 (2025).
[54] M. D. Louwerse and D. A. Sivak, Information thermodynamics of the transition-path ensemble, Phys. Rev. Lett. **128**, 170602 (2022).
[55] A. Kolchinsky, I. Marvian, C. Gokler, Z.-W. Liu, P. Shor, O. Shtanko, K. Thompson, D. Wolpert, and S. Lloyd, Maximizing free energy gain, Entropy **27**, 91 (2025).
[56] D. Lucente, A. Manacorda, A. Plati, A. Sarracino, and M. Baldovin, Optimal control of an electromechanical energy harvester, Entropy **27**, 268 (2025).
[57] K. S. Olsen, R. Goerlich, Y. Roichman, and H. Löwen, Harnessing non-equilibrium forces to optimize work extraction, Nat. Commun. **16**, 11031 (2025).
[58] M. Ribezzi-Crivellari and F. Ritort, Large work extraction and the Landauer limit in a continuous Maxwell demon, Nat. Phys. **15**, 660 (2019).
[59] G. Paneru, D. Y. Lee, T. Tlusty, and H. K. Pak, Lossless Brownian information engine, Phys. Rev. Lett. **120**, 020601 (2018).
[60] S. Still, Thermodynamic cost and benefit of memory, Phys. Rev. Lett. **124**, 050601 (2020).
[61] S. Dago and L. Bellon, Dynamics of information erasure and extension of Landauer's bound to fast processes, Phys. Rev. Lett. **128**, 070604 (2022).
[62] S. Dago, S. Ciliberto, and L. Bellon, Adiabatic computing for optimal thermodynamic efficiency of information processing, Proc. Natl. Acad. Sci. U.S.A. **120**, e2301742120 (2023).
[63] A. Archambault, C. Crauste-Thibierge, S. Ciliberto, and L. Bellon, Inertial effects in discrete sampling information engines, Europhys. Lett. **148**, 41002 (2024).
[64] J. Sanders, M. Baldovin, and P. Muratore-Ginanneschi, Optimal control of underdamped systems: An analytic approach, J. Stat. Phys. **191**, 117 (2024).
[65] J. Sanders, M. Baldovin, and P. Muratore-Ginanneschi, Minimal work protocols for inertial particles in nonharmonic traps, Phys. Rev. E **111**, 034127 (2025).
[66] J. Bechhoefer, *Control Theory for Physicists* (Cambridge University Press, Cambridge, England, 2021), https://www.cambridge.org/core/books/control-theory-for-physicists/21AFE5D6C475D1B44BCF9B8536338D98.
[67] K. H. Kim and H. Qian, Entropy production of Brownian macromolecules with inertia, Phys. Rev. Lett. **93**, 120602 (2004).
[68] P. Malgaretti and H. Stark, Szilard engines and information-based work extraction for active systems, Phys. Rev. Lett. **129**, 228005 (2022).
[69] L. Cocconi and L. Chen, Efficiency of an autonomous, dynamic information engine operating on a single active particle, Phys. Rev. E **110**, 014602 (2024).
[70] A. Datta, P. Pietzonka, and A. C. Barato, Second law for active heat engines, Phys. Rev. X **12**, 031034 (2022).
[71] J. S. Lee, J.-M. Park, and H. Park, Brownian heat engine with active reservoirs, Phys. Rev. E **102**, 032116 (2020).
[72] R. Garcia-Millan, J. Schüttler, M. E. Cates, and S. A. M. Loos, Optimal closed-loop control of active particles and a minimal information engine, Phys. Rev. Lett. **135**, 088301 (2025).
[73] A. Patrón Castro, https://github.com/apatroncastro/Harnessing-higher-dimensional-fluctuations-in-an-information-engine.

Supplemental Material for "Harnessing higher-dimensional fluctuations in an information engine"

I. ZERO-WORK CONDITION AND OPTIMAL FEEDBACK RULE

Here we derive the zero-work condition and the optimal feedback rule (10) for a pure information engine in d-dimensions, as described in *Multidimensional information engine* in the main text. We recall from there that work is defined as the change in the total potential due to the update of the center of the harmonic trap (8a).

The zero-work (pure information engine) condition is thus

$$W_{n+1} = 0 \iff |\boldsymbol{r}_{n+1} - \boldsymbol{\lambda}_{n^+ +1}| = |\boldsymbol{r}_{n+1} - \boldsymbol{\lambda}_{n^+}| \ . \tag{I.1}$$

Thus $\boldsymbol{\lambda}_{n^+ +1}$ lies on a hypersphere centered at $\boldsymbol{r}_{n+1}$ with radius $|\boldsymbol{r}_{n+1} - \boldsymbol{\lambda}_{n^+}|$. Contrary to the one-dimensional information engine from [1], here there are infinitely many possible positions for the updated trap center $\boldsymbol{\lambda}_{n^+ +1}$. In the following, we choose the feedback rule for $\boldsymbol{\lambda}_{n^+ +1}$ to maximize the extracted gravitational free energy.

Given a fixed trap center $\boldsymbol{\lambda}$, the equilibrium free energy is

$$F(\boldsymbol{\lambda}) \equiv \langle V(\boldsymbol{r}, \boldsymbol{\lambda}) + \log \pi(\boldsymbol{r}|\boldsymbol{\lambda}) \rangle_{\pi(\boldsymbol{r}|\boldsymbol{\lambda})} \ , \tag{I.2}$$

for canonical equilibrium distribution

$$\pi(\boldsymbol{r}|\boldsymbol{\lambda}) \equiv \frac{1}{\mathcal{Z}(\boldsymbol{\lambda})} \, \mathrm{e}^{-V(\boldsymbol{r}, \boldsymbol{\lambda})} \tag{I.3}$$

and the corresponding partition function

$$\mathcal{Z}(\boldsymbol{\lambda}) \equiv \int \mathrm{d}\boldsymbol{r} \ \ \mathrm{e}^{-V(\boldsymbol{r}, \boldsymbol{\lambda})} \ , \tag{I.4}$$

which is a Gaussian integral since the potential (4) is harmonic. Combining Eqs. (I.2)-(I.4) results in

$$F(\boldsymbol{\lambda}) = -\log \mathcal{Z}(\boldsymbol{\lambda}) \tag{I.5a}$$

$$= \boldsymbol{\delta}_{\mathbf{g}}^{\top} \boldsymbol{\lambda} + F(\mathbf{0}) \tag{I.5b}$$

$$= \delta_{\mathrm{g}} \lambda^{(z)} + F(\mathbf{0}) \ , \tag{I.5c}$$

with $F(\mathbf{0})$ the free energy for $\boldsymbol{\lambda} = 0$. Thus, the stored equilibrium free energy between measurements is

$$\langle \Delta F \rangle = \langle F(\boldsymbol{\lambda}_{n^+ +1}) - F(\boldsymbol{\lambda}_{n^+}) \rangle \tag{I.6a}$$

$$= \delta_{\mathrm{g}} \left\langle \lambda^{(z)}_{n^+ +1} - \lambda^{(z)}_{n^+} \right\rangle \ . \tag{I.6b}$$

This only depends on the trap center's z-component; maximizing this z-component means the updated trap center lies at the top of the hypersphere defined via (I.1). Hence, the optimal feedback rule is

$$\boldsymbol{\lambda}_{n^+ +1} = \boldsymbol{r}_{n+1} + |\boldsymbol{r}_{n+1} - \boldsymbol{\lambda}_{n^+}| \, \hat{\boldsymbol{z}} \ , \tag{I.7}$$

for unit vector $\hat{\boldsymbol{z}}$ in the z-direction.

II. HIGH-SAMPLING-FREQUENCY LIMIT

Here we derive Eq. (13) from *Optimal performance* in the main text, the analytical expression for the output power $P_{\mathrm{net}}^{\mathrm{HF}}$ in the high-sampling-frequency limit.

For sufficiently high sampling frequency f_{s}, $\boldsymbol{\lambda}$ evolves almost continuously in time. We first consider the differential change $\mathrm{d}\lambda^{(z)}_{n^+ +1} \equiv \lambda^{(z)}_{n^+ +1} - \lambda^{(z)}_{n^+}$ of $\lambda^{(z)}$, given differential change $\mathrm{d}\boldsymbol{r}_{n+1} \equiv \boldsymbol{r}_{n+1} - \boldsymbol{r}_n$ of the bead position. The feedback rule (10) and feedback cooling of the transverse degrees of freedom (dictating $\lambda^{(i)}_{n^+} = x^{(i)}_n$) gives

$$\mathrm{d}\lambda^{(z)}_{n^+ +1} = \mathrm{d}z_{n+1} - L_n + \sqrt{(L_n - \mathrm{d}z_{n+1})^2 + \sum_{j=1}^{d-1} \left(\mathrm{d}x^{(j)}_{n+1} \right)^2} \ , \tag{II.1}$$

for trap-bead displacement $L_n \equiv \lambda^{(z)}_{n^+} - z_n$ after the feedback. Since $\boldsymbol{\lambda}_{n^+}$ always lies at the top of the hypersphere defined by the zero-work condition, $L_n \geq 0$. For sufficiently short sampling time t_s, the displacements $\mathrm{d}z_{n+1}$ and $\mathrm{d}x^{(i)}_{n+1}$ are small and of the same order: $\mathrm{d}z_{n+1}, \mathrm{d}x^{(i)}_{n+1} \sim O(\sqrt{t_\mathrm{s}})$. Taylor expanding Eq. (II.1) up to leading orders in $\mathrm{d}z_{n+1}$ and $\mathrm{d}x^{(i)}_{n+1}$ yields z trap-center displacement

$$\mathrm{d}\lambda^{(z)}_{n^+ +1} \approx \frac{1}{2L_n} \sum_{i=1}^{d-1} \left(\mathrm{d}x^{(i)}_{n+1}\right)^2 \tag{II.2a}$$

$$\approx \frac{1}{L_n} \sum_{i=1}^{d-1} \left(\mathrm{d}W^{(i)}_t\right)^2 \tag{II.2b}$$

$$= \frac{d-1}{L_n}\,\mathrm{d}t \ , \tag{II.2c}$$

and hence vertical velocity

$$\dot{\lambda}^{(z)}_{n^+ +1} \equiv \frac{\mathrm{d}\lambda^{(z)}_{n^+ +1}}{\mathrm{d}t} \tag{II.3a}$$

$$= \frac{d-1}{L_n} \ . \tag{II.3b}$$

In Eq. (II.2b), we employed the bounded quadratic variation formula $(\mathrm{d}W_t)^2 = \mathrm{d}t$ for Wiener processes, which follows from Ito's lemma [2].

To proceed further, we determine the steady-state distribution $p_\mathrm{ss}(L)$ for the trap-bead displacements L_n. Combining Eqs. (II.2b) and (5) gives the stochastic differential equation for L_n:

$$\mathrm{d}L_{n+1} \equiv L_{n+1} - L_n \tag{II.4a}$$

$$= \mathrm{d}\lambda^{(z)}_{n^+ +1} - \mathrm{d}z_{n+1} \tag{II.4b}$$

$$\approx (\delta_\mathrm{g} - L_n)\mathrm{d}t + \frac{1}{2L_n} \sum_{i=1}^{d-1} \left(\mathrm{d}W^{(i)}_t\right)^2 - \sqrt{2}\,\mathrm{d}W^{(z)}_t \ . \tag{II.4c}$$

Its corresponding distribution dynamically evolves according to the Fokker-Planck equation

$$\frac{\partial p}{\partial t} = \frac{\partial}{\partial L}\left[\left(L - \delta_\mathrm{g} - \frac{d-1}{L}\right)p + \frac{\partial p}{\partial L}\right] \ , \tag{II.5}$$

which has steady-state distribution

$$p_\mathrm{ss}(L) = \frac{1}{\mathcal{Z}_d(\delta_\mathrm{g})} L^{d-1}\,\mathrm{e}^{-L^2/2 + \delta_\mathrm{g} L} \ , \tag{II.6}$$

for partition function

$$\mathcal{Z}_d(\delta_\mathrm{g}) \equiv \int_0^\infty \mathrm{d}L\ L^{d-1}\,\mathrm{e}^{-L^2/2+\delta_\mathrm{g} L} \tag{II.7a}$$

$$= 2^{(d-3)/2}\left[\sqrt{2}\,\Gamma\left(\frac{d}{2}\right)\,{}_1F_1\left(\frac{d}{2}, \frac{1}{2}, \frac{\delta_\mathrm{g}^2}{2}\right) + 2\delta_\mathrm{g}\,\Gamma\left(\frac{1+d}{2}\right)\,{}_1F_1\left(\frac{1+d}{2}, \frac{3}{2}, \frac{\delta_\mathrm{g}^2}{2}\right)\right] \ . \tag{II.7b}$$

Here ${}_1F_1(a,b,c)$ is the confluent hypergeometric function of the first kind. This gives output power

$$P^\mathrm{HF}_\mathrm{net} = (d-1)\delta_\mathrm{g}\left\langle \frac{1}{L} \right\rangle \tag{II.8a}$$

$$= (d-1)\delta_\mathrm{g} \frac{\mathcal{Z}_{d-1}(\delta_\mathrm{g})}{\mathcal{Z}_d(\delta_\mathrm{g})} \ . \tag{II.8b}$$

and vertical velocity

$$\langle v_z \rangle^{\mathrm{HF}} = (d-1)\frac{\mathcal{Z}_{d-1}(\delta_{\mathrm{g}})}{\mathcal{Z}_d(\delta_{\mathrm{g}})} \ , \tag{II.9}$$

corresponding to Eq. (13) from the main text.

Given that the velocity monotonically decreases with δ_{g}, the maximum is attained at $\delta_{\mathrm{g}} = 0$,

$$\max_{\delta_{\mathrm{g}}} \left[\langle v_z \rangle^{\mathrm{HF}} \right] = (d-1)\frac{\mathcal{Z}_{d-1}(0)}{\mathcal{Z}_d(0)} \tag{II.10a}$$

$$= \frac{d-1}{\sqrt{2}} \frac{\Gamma\left(\frac{d-1}{2}\right)}{\Gamma\left(\frac{d}{2}\right)} \ . \tag{II.10b}$$

This expression holds even for $d \to 1$, giving $\sqrt{2/\pi}$. In the $\delta_g \to \infty$, the integral from (II.7a) can be approximated using Laplace's method [3], giving the asymptotic limit

$$\mathcal{Z}_d(\delta_{\mathrm{g}}) \sim \sqrt{2\pi}\, \delta_{\mathrm{g}}^d \, \mathrm{e}^{\delta_{\mathrm{g}}^2/2} \ . \tag{II.11}$$

This expression is employed in the main text to obtain the asymptotic value $d-1$ for the output power.

III. LOW-SAMPLING-FREQUENCY LIMIT

Here we derive an analytical expression for the output power $P_{\mathrm{net}}^{\mathrm{LF}}$ in the low-sampling-frequency limit.

When the sampling frequency f_{s} is small, between successive feedback steps the bead-position distribution equilibrates, giving the canonical equilibrium distribution

$$p_{\mathrm{eq}}(\boldsymbol{r};\boldsymbol{\lambda}) = \mathcal{N}_d(\boldsymbol{r}|\, \boldsymbol{\lambda} - \mathbf{g}; 1) \tag{III.1a}$$

$$= \mathcal{N}_1(z|\, \lambda^{(z)} - \delta_{\mathrm{g}}; 1) \prod_{i=1}^{d-1} \mathcal{N}_1(x^{(i)}|\, \lambda^{(i)}; 1) \ . \tag{III.1b}$$

where $\mathcal{N}_d(\boldsymbol{x}|\, \boldsymbol{\mu}; \sigma^2)$ denotes a d-dimensional normal (Gaussian) distribution over $\boldsymbol{x}$, with mean $\boldsymbol{\mu}$ and variance σ^2. Combining this and the feedback rule (10) gives the average equilibrium free-energy storage per feedback step,

$$\langle \Delta F \rangle_{\mathrm{eq}} = \delta_{\mathrm{g}} \int_{\mathbb{R}_d} \mathrm{d}\boldsymbol{r} \left[z - \lambda^{(z)} + \sqrt{(z-\lambda^{(z)})^2 + \sum_{j=1}^{d-1} (x^{(j)} - \lambda^{(j)})^2} \right] p_{\mathrm{eq}}(\boldsymbol{r};\boldsymbol{\lambda}) \tag{III.2a}$$

$$= \delta_{\mathrm{g}} \int_{\mathbb{R}_d} \mathrm{d}z \left[\prod_{i=1}^{d-1} \mathrm{d}x^{(i)}\ \mathcal{N}_1(x^{(i)}|\, \lambda^{(i)}; 1) \right] \left[z - \lambda^{(z)} + \sqrt{(z-\lambda^{(z)})^2 + \sum_{j=1}^{d-1} (x^{(j)} - \lambda^{(j)})^2} \right] \mathcal{N}_1(z|\, \lambda^{(z)} - \delta_{\mathrm{g}}; 1) \tag{III.2b}$$

$$= -\delta_{\mathrm{g}}^2 + \frac{\delta_{\mathrm{g}}\ 2^{(1-d)/2}}{\sqrt{\pi}\, \Gamma\left(\frac{d-1}{2}\right)} \int_{-\infty}^{+\infty} \mathrm{d}\tilde{z} \int_0^{+\infty} \mathrm{d}r\ r^{d-2} \sqrt{\tilde{z}^2 + r^2}\ \exp\left\{ -\frac{r^2}{2} - \frac{(z+\delta_{\mathrm{g}})^2}{2} \right\} \ . \tag{III.2c}$$

In Eq. (III.2c), we made two changes of variables: (i) $\tilde{z} = z - \lambda^{(z)}$ and (ii) change to spherical coordinates for the $d-1$ perpendicular degrees of freedom. Therefore, in the limit of low sampling frequency the output power is

$$P_{\mathrm{net}}^{\mathrm{LF}} = f_{\mathrm{s}} \langle \Delta F \rangle_{\mathrm{eq}} \ . \tag{III.3}$$

This gives the gray dashed diagonal lines in Fig. 3.

IV. STEADY STATES FOR ARBITRARY SAMPLING FREQUENCY

Here we provide the details for the semi-analytical method employed to obtain the output power P_{net} for arbitrary sampling frequencies f_{s} in arbitrary $d > 1$ dimensions, which we employed for the solid red curve in Fig. 3.

To determine the output power for arbitrary sampling frequency, we follow the reasoning of [1]. First, we derive a self-consistency equation for the steady-state position distribution as a function of sampling frequency, which we evaluate numerically. The joint transition probability from bead position $\boldsymbol{r}_n$ and trap center $\boldsymbol{\lambda}_{n^+}$ to $\boldsymbol{r}_{n+1}$ and $\boldsymbol{\lambda}_{n^+ +1}$ is

$$p(\boldsymbol{r}_{n+1}, \boldsymbol{\lambda}_{n^+ +1} | \, \boldsymbol{r}_n, \boldsymbol{\lambda}_{n^+}) = \underbrace{p_{\boldsymbol{\lambda}}(\boldsymbol{\lambda}_{n^+ +1} | \, \boldsymbol{r}_{n+1}, \boldsymbol{\lambda}_{n^+})}_{\text{feedback}} \, \underbrace{p_{\boldsymbol{r}}(\boldsymbol{r}_{n+1} | \, \boldsymbol{r}_n, \boldsymbol{\lambda}_{n^+})}_{\text{propagator}} \, . \tag{IV.1}$$

The bead-position propagator $p_{\boldsymbol{r}}(\boldsymbol{r}_{n+1} | \, \boldsymbol{r}_n, \boldsymbol{\lambda}_{n^+})$ for diffusion in a harmonic potential is given by the generator for a d-dimensional Ornstein-Uhlenbeck process,

$$p_{\boldsymbol{r}}(\boldsymbol{r}_{n+1} | \, \boldsymbol{r}_n, \boldsymbol{\lambda}_{n^+}) = \mathcal{N}_d(\boldsymbol{r}_{n+1} | \, \boldsymbol{\mu}(\boldsymbol{r}_n, \boldsymbol{\lambda}_{n^+}, t_\mathrm{s}); \sigma(t_\mathrm{s})^2) \, , \tag{IV.2}$$

with mean

$$\boldsymbol{\mu}(\boldsymbol{r}_n, \boldsymbol{\lambda}_{n^+}, t_\mathrm{s}) \equiv \mathrm{e}^{-t_\mathrm{s}} \, \boldsymbol{r}_n + (1 - \mathrm{e}^{-t_\mathrm{s}})(\boldsymbol{\lambda}_{n^+} - \boldsymbol{\delta}_\mathbf{g}) \, , \tag{IV.3}$$

and standard deviation $\sigma(t_\mathrm{s}) \equiv \sqrt{1 - \mathrm{e}^{-2t_\mathrm{s}}}$ at time t_s. The propagator $p_{\boldsymbol{\lambda}}(\boldsymbol{\lambda}_{n^+ +1} | \, \boldsymbol{r}_{n+1}, \boldsymbol{\lambda}_{n^+})$ for the trap center follows from the feedback rule (10):

$$p_{\boldsymbol{\lambda}}(\boldsymbol{\lambda}_{n^+ +1} | \, \boldsymbol{r}_{n+1}, \boldsymbol{\lambda}_{n^+}) = \delta_d(\boldsymbol{\lambda}_{n^+ +1} - \boldsymbol{r}_{n+1} - |\boldsymbol{r}_{n+1} - \boldsymbol{\lambda}_{n^+}| \hat{\boldsymbol{z}}) \, . \tag{IV.4}$$

Here, $\delta_d(\cdot)$ denotes the d-dimensional Dirac delta function. Changing variables to relative coordinates

$$\boldsymbol{r}^\mathrm{r}_{n^+} \equiv \boldsymbol{r}_{n+1} - \boldsymbol{\lambda}_{n^+} \tag{IV.5a}$$

$$\boldsymbol{r}^\mathrm{r}_{n} \equiv \boldsymbol{r}_{n} - \boldsymbol{\lambda}_{n^+} \tag{IV.5b}$$

yields

$$\begin{aligned}
p_{\boldsymbol{r}}(\boldsymbol{r}^\mathrm{r}_{n^+} \, | \, \boldsymbol{r}_n, \boldsymbol{\lambda}_{n^+}) &= \int_{\mathbb{R}_d} \mathrm{d}\boldsymbol{r}_{n+1} \; \delta_d(\boldsymbol{r}_{n+1} - \boldsymbol{r}^\mathrm{r}_{n^+} - \boldsymbol{\lambda}_{n^+}) \; p_{\boldsymbol{r}}(\boldsymbol{r}_{n+1} | \boldsymbol{r}_n, \boldsymbol{\lambda}_n) && \text{(IV.6a)} \\
&= \mathcal{N}_d(\boldsymbol{r}^\mathrm{r}_{n^+} \, | \, \boldsymbol{\mu}(\boldsymbol{r}^\mathrm{r}_n, \mathbf{0}, t_\mathrm{s}); \sigma(t_\mathrm{s})^2) && \text{(IV.6b)} \\
&\equiv p_1(\boldsymbol{r}^\mathrm{r}_{n^+} \, | \, \boldsymbol{r}^\mathrm{r}_n) && \text{(IV.6c)} \\
p_{\boldsymbol{\lambda}}(\boldsymbol{r}^\mathrm{r}_{n+1} | \boldsymbol{r}_{n+1}, \boldsymbol{\lambda}_{n^+}) &= \int_{\mathbb{R}_d} \mathrm{d}\boldsymbol{\lambda}_{n^+ +1} \; \delta_d(\boldsymbol{\lambda}_{n^+ +1} - \boldsymbol{r}_{n+1} + \boldsymbol{r}^\mathrm{r}_{n+1}) \; p_{\boldsymbol{\lambda}}(\boldsymbol{\lambda}_{n^+ +1} | \boldsymbol{r}_{n+1}, \boldsymbol{\lambda}_n) && \text{(IV.6d)} \\
&= \delta_d(\boldsymbol{r}^\mathrm{r}_{n+1} + \, | \, \boldsymbol{r}^\mathrm{r}_{n^+} | \hat{\boldsymbol{z}}) && \text{(IV.6e)} \\
&\equiv p_2(\boldsymbol{r}^\mathrm{r}_{n+1} \, | \, \boldsymbol{r}^\mathrm{r}_{n^+}) \, . && \text{(IV.6f)}
\end{aligned}$$

The steady-state solutions satisfy the self-consistent integral equations

$$\pi_+ \left(\boldsymbol{r}^\mathrm{r}_{n^+}\right) = \int_{\mathbb{R}_d} \mathrm{d}\boldsymbol{u} \, \underbrace{\int_{\mathbb{R}_d} \mathrm{d}\boldsymbol{v} \, p_1 \left(\boldsymbol{r}^\mathrm{r}_{n^+} \, | \, \boldsymbol{v}\right) p_2(\boldsymbol{v} \, | \, \boldsymbol{u})}_{\equiv T\left(\boldsymbol{r}^\mathrm{r}_{n^+} | \boldsymbol{u}\right)} \pi_+(\boldsymbol{u}) \tag{IV.7a}$$

$$\pi \left(\boldsymbol{r}^\mathrm{r}_{n}\right) = \int_{\mathbb{R}_d} \mathrm{d}\boldsymbol{v} \, \underbrace{\int_{\mathbb{R}_d} \mathrm{d}\boldsymbol{u} \, p_2 \left(\boldsymbol{r}^\mathrm{r}_{n} \, | \, \boldsymbol{u}\right) p_1(\boldsymbol{u} \, | \, \boldsymbol{v})}_{\equiv \tilde{T}\left(\boldsymbol{r}^\mathrm{r}_{n} | \boldsymbol{v}\right)} \pi(\boldsymbol{v}) \, , \tag{IV.7b}$$

where $\boldsymbol{u}$ and $\boldsymbol{v}$ are d-dimensional vectors of dummy variables of integration, and the propagators are

$$\begin{aligned}
T \left(\boldsymbol{r}^\mathrm{r}_{n^+} \, | \, \boldsymbol{u}\right) &= \mathcal{N}_d\Big(\boldsymbol{r}^\mathrm{r}_{n^+} \, \Big| \, \boldsymbol{\mu}(-|\boldsymbol{u}| \hat{\boldsymbol{z}}, \mathbf{0}, t_\mathrm{s}); \sigma(t_\mathrm{s})^2\Big) && \text{(IV.8a)} \\
&= \mathcal{N}_1\Big(z^\mathrm{r}_{n^+} \Big| \; \mu_z(-|\boldsymbol{u}|, 0, t_\mathrm{s}); \sigma(t_\mathrm{s})^2\Big) \prod_{i=1}^{d-1} \mathcal{N}_1 \left(x^{(i),\mathrm{r}}_{n^+} \, \Big| \, 0; \sigma(t_\mathrm{s})^2\right) && \text{(IV.8b)} \\
\tilde{T} \left(\boldsymbol{r}^\mathrm{r}_{n} \, | \, \boldsymbol{v}\right) &= \int_{\mathbb{R}_d} \mathrm{d}\boldsymbol{u} \; \delta_d(\boldsymbol{r}^\mathrm{r}_n + |\boldsymbol{u}|) \, \mathcal{N}_d\Big(\boldsymbol{u} \, \Big| \, \boldsymbol{\mu}(\boldsymbol{v}, \mathbf{0}, t_\mathrm{s}); \sigma(t_\mathrm{s})^2\Big) && \text{(IV.8c)} \\
&= \left[\int_{|\boldsymbol{\omega}|=1} \mathrm{d}\boldsymbol{\omega} \; \mathcal{N}_d\Big(- z^\mathrm{r}_n \boldsymbol{\omega} \, \Big| \, \boldsymbol{\mu}(\boldsymbol{v}, \mathbf{0}, t_\mathrm{s}); \sigma(t_\mathrm{s})^2\Big)\right] (-z^\mathrm{r}_n)^{d-1} \, \Theta(-z^\mathrm{r}_n) \prod_{i=1}^{d-1} \delta_1 \left(x^{(i),\mathrm{r}}_n\right) \, . && \text{(IV.8d)}
\end{aligned}$$

In principle, one can numerically solve for the steady-state distributions (IV.7) by discretizing the propagator $T\left(\boldsymbol{r}^{\mathrm{r}}_{n^+} \mid \boldsymbol{u}\right)$ in $\boldsymbol{r}^{\mathrm{r}}_{n^+}$ and $\boldsymbol{u}$ and the propagator $\tilde{T}\left(\boldsymbol{r}^{\mathrm{r}}_{n} \mid \boldsymbol{v}\right)$ in $\boldsymbol{r}^{\mathrm{r}}_{n}$ and $\boldsymbol{v}$. The corresponding eigenvectors with unit eigenvalue give the distributions $\pi_+(\boldsymbol{r}^{\mathrm{r}}_{n^+})$ and $\pi(\boldsymbol{r}^{\mathrm{r}}_{n})$, respectively.

Determining the eigenvalues of the propagators $T\left(\boldsymbol{r}^{\mathrm{r}}_{n^+} \mid \boldsymbol{u}\right)$ and $\tilde{T}\left(\boldsymbol{r}^{\mathrm{r}}_{n} \mid \boldsymbol{v}\right)$ is in practice often challenging, since it involves the discretization of d-dimensional integrals on a sufficiently fine grid in order to achieve high accuracy, a task that becomes increasingly computationally expensive as the dimensionality increases. In the following, we reduce the d-dimensional integral eigenvalue problem (IV.7) to an effective one-dimensional problem. We note that the propagators $T\left(\boldsymbol{r}^{\mathrm{r}}_{n^+} \mid \boldsymbol{u}\right)$ and $\tilde{T}\left(\boldsymbol{r}^{\mathrm{r}}_{n} \mid \boldsymbol{v}\right)$ from Eqs. (IV.8) each factorize into the product of a function depending only on the transverse degrees of freedom $x^{(i)},\ i=1,...,d-1$ and a function depending only on the parallel (z) component and the integration variables $\boldsymbol{u}$ and $\boldsymbol{v}$. Following this, inserting Eqs. (IV.8) into Eqs. (IV.7) shows that the steady-state distributions obey a principle of separation of variables:

$$\pi_+(\boldsymbol{r}^{\mathrm{r}}_{n^+}) = \prod_{i=1}^{d-1} \mathcal{N}_1\left(x^{(i),\mathrm{r}}_{n^+} \,\middle|\, 0; \sigma(t_{\mathrm{s}})^2\right) \underbrace{\int_{\mathbb{R}_d} \mathrm{d}\boldsymbol{u}\ \mathcal{N}_1\Big(z^{\mathrm{r}}_{n^+} \,\Big|\, \mu_z(-|\boldsymbol{u}|,0,t_{\mathrm{s}}); \sigma(t_{\mathrm{s}})^2\Big)\pi_+(\boldsymbol{u})}_{\equiv g_+(z^{\mathrm{r}}_{n^+})} \tag{IV.9a}$$

$$\pi(\boldsymbol{r}^{\mathrm{r}}_{n}) = (-z^{\mathrm{r}}_{n})^{d-1}\,\Theta(-z^{\mathrm{r}}_{n}) \prod_{i=1}^{d-1} \delta_1\left(x^{(i),\mathrm{r}}_{n}\right) \underbrace{\int_{\mathbb{R}_d} \mathrm{d}\boldsymbol{v} \int_{|\boldsymbol{\omega}|=1} \mathrm{d}\boldsymbol{\omega}\ \mathcal{N}_d\Big(-z^{\mathrm{r}}_{n}\boldsymbol{\omega} \,\Big|\, \boldsymbol{\mu}(\boldsymbol{v},\boldsymbol{0},t_{\mathrm{s}}); \sigma(t_{\mathrm{s}})^2\Big)\pi(\boldsymbol{v})}_{\equiv g(z^{\mathrm{r}}_{n})}, \tag{IV.9b}$$

for unknown functions $g_+(z^{\mathrm{r}}_{n^+})$ and $g(z^{\mathrm{r}}_{n})$. Inserting Eqs. (IV.9) into the definitions of $g_+(z^{\mathrm{r}}_{n^+})$ and $g(z^{\mathrm{r}}_{n})$ gives

$$g_+(z^{\mathrm{r}}_{n^+}) = \int_{\mathbb{R}_d} \mathrm{d}\boldsymbol{u}\ \mathcal{N}_1\Big(z^{\mathrm{r}}_{n^+} \,\Big|\, \mu_z(-|\boldsymbol{u}|,0,t_{\mathrm{s}}); \sigma(t_{\mathrm{s}})^2\Big)\ g_+(u_z) \prod_{i=1}^{d-1} \mathcal{N}_1\left(u^{(i)} \,\middle|\, 0; \sigma(t_{\mathrm{s}})^2\right) \tag{IV.10a}$$

$$= \int_{\mathbb{R}} \mathrm{d}u_z \underbrace{\prod_{i=1}^{d-1} \left[\int_{\mathbb{R}} \mathrm{d}u^{(i)} \mathcal{N}_1\left(u^{(i)} \,\middle|\, 0; \sigma(t_{\mathrm{s}})^2\right)\right] \mathcal{N}_1\Big(z^{\mathrm{r}}_{n^+} \,\Big|\, \mu_z(-|\boldsymbol{u}|,0,t_{\mathrm{s}}); \sigma(t_{\mathrm{s}})^2\Big)}_{\equiv\ T_{\mathrm{eff}}(z^{\mathrm{r}}_{n^+}|u_z)}\ g_+(u_z) \tag{IV.10b}$$

$$g(z^{\mathrm{r}}_{n}) = \int_{\mathbb{R}_d} \mathrm{d}\boldsymbol{v} \int_{\mathbb{R}_d} \mathrm{d}\boldsymbol{\omega}\ \delta_d(|\boldsymbol{\omega}|-1)\,\mathcal{N}_d\Big(-z^{\mathrm{r}}_{n}\boldsymbol{\omega} \,\Big|\, \boldsymbol{\mu}(\boldsymbol{v},\boldsymbol{0},t_{\mathrm{s}}); \sigma(t_{\mathrm{s}})^2\Big)\ g(v_z)\,|v_z|^{d-1}\,\Theta(-v_z) \prod_{i=1}^{d-1} \delta_1\left(v^{(i)}\right) \tag{IV.10c}$$

$$= \int_{\mathbb{R}} \mathrm{d}v_z \underbrace{\int_{|\boldsymbol{\omega}|=1} \mathrm{d}\boldsymbol{\omega}\ \mathcal{N}_1\Big(-z^{\mathrm{r}}_{n}\omega_z \,\Big|\, \mu_z(v_z,0,t_{\mathrm{s}}); \sigma(t_{\mathrm{s}})^2\Big) \prod_{i=1}^{d-1} \mathcal{N}_1\Big(-z^{\mathrm{r}}_{n}\omega^{(i)} \,\Big|\, 0; \sigma(t_{\mathrm{s}})^2\Big) |v_z|^{d-1}\Theta(-v_z)}_{\equiv\ \tilde{T}_{\mathrm{eff}}(z^{\mathrm{r}}_{n}|v_z)}\ g(v_z)\ . \tag{IV.10d}$$

Hence, the functions $g_+(z^{\mathrm{r}}_{n^+})$ and $g(z^{\mathrm{r}}_{n})$ satisfy the effective one-dimensional eigenvalue problems

$$g_+(z^{\mathrm{r}}_{n^+}) = \int_{\mathbb{R}} \mathrm{d}u\ T_{\mathrm{eff}}(z^{\mathrm{r}}_{n^+}|u)\ g_+(u) \tag{IV.11a}$$

$$g(z^{\mathrm{r}}_{n}) = \int_{\mathbb{R}} \mathrm{d}v\ \tilde{T}_{\mathrm{eff}}(z^{\mathrm{r}}_{n}|v)\ g(v)\ . \tag{IV.11b}$$

The factorisation from Eq. (IV.9) can be understood on physical grounds, stemming from the feedback-cooling protocol (10) in the transverse degrees of freedom $(\lambda^{(1)},\lambda^{(2)},...\lambda^{(d-1)})$. On the one hand, since $\lambda^{(i)}_{n^+ +1} = x_{n+1}$, or, more generally, $\lambda^{(i)}_{n^+} = x_n\ \forall n$, the probability distribution $\pi^{(i)}\left(x^{(i),\mathrm{r}}_{n}\right)$ (after moving the trap center) for the relative displacements $x^{(i),\mathrm{r}}_{n} = x^{(i)}_{n} - \lambda^{(i)}_{n^+}$ is a Dirac-delta distribution centered at the origin, $\pi^{(i)}\left(x^{(i),\mathrm{r}}_{n}\right) = \delta_1\left(x^{(i),\mathrm{r}}_{n}\right)$. On the other hand, the bead's transverse coordinates $x^{(i)}_{n}$ subsequently evolve according to the discrete Langevin equation (5),

$$x^{(i)}_{n+1} = \mathrm{e}^{-t_{\mathrm{s}}} x^{(i)}_{n} + (1-\mathrm{e}^{-t_{\mathrm{s}}})\lambda^{(i)}_{n^+} + \sigma(t_{\mathrm{s}})\nu^{(i)}_{n}, \quad i=1,...,d-1\ . \tag{IV.12}$$

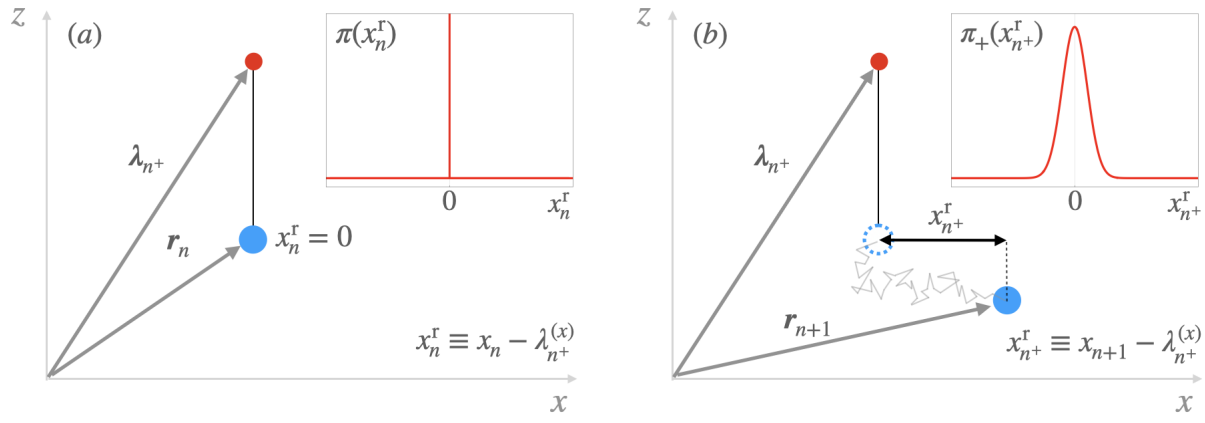

FIG. 1. Dynamics of the transverse degrees of freedom (x, for a 2D engine), justifying the factorisation (IV.9) for the steady-state distributions $\pi_+(\boldsymbol{r}_{n^+}^{\mathrm{r}})$ and $\pi(\boldsymbol{r}_n^{\mathrm{r}})$. (a) Immediately after a trap update, the bead and the trap have the same x-component; the distribution of relative displacements then reduces to a Dirac delta (inset). (b) After a time t_{s}, the bead's position is distributed according to the discrete Langevin equation (5). The relative bead-trap displacement along x is drawn from a Gaussian distribution with zero mean and standard deviation $\sigma(t_{\mathrm{s}})$ (inset).

Invoking once again the feedback rule $\lambda_{n^+}^{(i)} = x_n^{(i)}$ from Eq. (10), the Langevin equation reduces to

$$x_{n+1}^{(i)} - \lambda_{n^+}^{(i)} = \sigma(t_{\mathrm{s}})\nu_n^{(i)} \; ; \tag{IV.13}$$

hence, the bead-trap displacement $x_{n^+}^{(i),\mathrm{r}} = x_{n+1}^{(i)} - \lambda_{n^+}^{(i)}$ is drawn from a Gaussian distribution with null mean and standard deviation $\sigma(t_{\mathrm{s}})$, i.e., $\pi_+^{(i)}(x_{n^+}^{(i),\mathrm{r}}) = \mathcal{N}_1\left(x_{n^+}^{(i),\mathrm{r}} \middle| 0; \sigma(t_{\mathrm{s}})^2\right)$. Figure 1 illustrates this reasoning.

In Fig. 3, we consider the $d=2$ case, for which the effective propagators become

$$T_{\mathrm{eff}}(z_{n^+}^{\mathrm{r}} \,|\, u) = \int_{-\infty}^{+\infty} \mathrm{d}u' \; \mathcal{N}_1\left(z_{n^+}^{\mathrm{r}} \,\middle|\, -\mathrm{e}^{-t_{\mathrm{s}}}\sqrt{(u)^2 + (u')^2} - (1-\mathrm{e}^{-t_{\mathrm{s}}})\delta_{\mathrm{g}}; \sigma(t_{\mathrm{s}})^2\right) \cdot \mathcal{N}_1\left(u' \,|\, 0; \sigma(t_{\mathrm{s}})^2\right), \tag{IV.14a}$$

$$\tilde{T}_{\mathrm{eff}}(z_n^{\mathrm{r}} \,|\, v) = |v|\,\Theta(-v)\; \mathcal{N}_1\left(z_n^{\mathrm{r}} \,|\, 0; \sigma(t_{\mathrm{s}})^2\right)\; \mathcal{N}_1\left(\mathrm{e}^{-t_{\mathrm{s}}} v - (1-\mathrm{e}^{-t_{\mathrm{s}}})\delta_{\mathrm{g}} \,|\, 0; \sigma(t_{\mathrm{s}})^2\right)\; I_0\left(\frac{z_n^{\mathrm{r}}}{\sigma(t_{\mathrm{s}})^2}[\mathrm{e}^{-t_{\mathrm{s}}} v - (1-\mathrm{e}^{-t_{\mathrm{s}}})\delta_{\mathrm{g}}]\right), \tag{IV.14b}$$

with $I_0(\cdot)$ the modified Bessel function of the first kind of order 0. To obtain the semi-analytical results in Fig. 3, we discretized the effective propagator $T_{\mathrm{eff}}(z_{n^+}^{\mathrm{r}}|u)$ in a grid of $2,000 \times 2,000$ uniformly spaced points in the domain $z_{n^+}^{\mathrm{r}}, u \in [-20, 20]$. For the remaining propagator $\tilde{T}_{\mathrm{eff}}(z_n^{\mathrm{r}}|v)$, given the numerical instabilities of the modified Bessel function, we used a much finer grid of $50,000 \times 50,000$ points in the domain $z_n^{\mathrm{r}}, v \in [-20, 0]$.

V. HORIZONTAL THRESHOLD

Here we investigate whether it is more advantageous to exploit all such transverse fluctuations or only a subset, by computing the maximum output power P_{net} as a function of the radial threshold R for the transverse degrees of freedom, as briefly discussed in *Optimal performance* in the main text.

We study the dependence of the output power on R in the high-sampling-frequency limit, for which we have already shown that the performance is optimal. In this limit, the output power can be interpreted as the ratio of extracted work to the first-passage time required for the bead to reach the cylinder. Two competing effects arise as a function of the threshold R. On one hand, the extracted work per ratchet event increases with R: the larger the threshold, the greater the radius at which the zero-work condition is met, and thus the more work is extracted. On the other hand, the mean first-passage time also increases with R, since the bead must travel a greater distance before triggering a trap update.

For a nonzero feedback threshold R, the trap center is adjusted only once the bead position projected onto the transverse plane exceeds distance R from the trap center. For measurements at fixed time intervals τ, the output

power $P_{\rm net}$ is the ratio between the average gain $\langle \Delta F \rangle$ in stored gravitational free energy per ratchet event and the time between events:

$$P_{\rm net}(\tau, R) \equiv \frac{\langle \Delta F \rangle}{\tau} \tag{V.1a}$$

$$= \frac{\delta_{\rm g}}{\tau} \left\langle \lambda^{(z)}_{n^+ + 1} - \lambda^{(z)}_{n^+} \right\rangle \tag{V.1b}$$

$$= \frac{\delta_{\rm g}}{\tau} \left\langle z_{n+1} - \lambda^{(z)}_{n^+} + \sqrt{\left(z_{n+1} - \lambda^{(z)}_{n^+}\right)^2 + R^2} \right\rangle \ . \tag{V.1c}$$

In Eq. (V.1b), we employed the definition of $\langle \Delta F \rangle$ (9) and the feedback rule (11). Inserting the discrete Langevin equation (5) and the vertical distance $L_n \equiv \lambda^{(z)}_{n^+} - z_n \geq 0$ gives

$$P_{\rm net}(\tau, R) = \frac{\delta_{\rm g}}{\tau} \overline{\left\langle (1 - {\rm e}^{-\tau})(L_n - \delta_{\rm g}) - L_n + \sqrt{\left[(1 - {\rm e}^{-\tau})(L_n - \delta_{\rm g}) + \sqrt{1 - {\rm e}^{-2\tau}}\ \xi_n - L_n\right]^2 + R^2} \right\rangle} \ . \tag{V.2}$$

The overline indicates an average over noise realizations ξ_n drawn from a normal distribution of zero mean and unit variance.

In principle, one would also need to average over all possible times τ between ratchet events. The distribution of such times is the first-passage-time distribution for a bead starting at the origin, with an absorbing boundary at the surface of a $(d-1)$-dimensional hypersphere of radius R. Unfortunately, even for the simple case of harmonic confinement, obtaining the first-passage distribution is non-trivial, beyond the scope of this paper. To estimate the qualitative dependence of $P_{\rm net}$ on R, we approximate the first-passage distribution as a Dirac-delta centered at the mean first-passage time $\tau_{\rm MFP}$, obtained from the solution of the backward Fokker-Planck equation in $d-1$ dimensions,

$$-\boldsymbol{r}^\top \nabla \mathbb{T}(\boldsymbol{r}) + \nabla^2 \mathbb{T}(\boldsymbol{r}) = -1 \ , \tag{V.3}$$

with absorbing boundary condition

$$\mathbb{T}(|\boldsymbol{r}| = R) = 0 \ . \tag{V.4}$$

The mean first-passage time is then

$$\tau_{\rm MFP} = \mathbb{T}(\boldsymbol{0}) \ . \tag{V.5}$$

For $d=2$ this reduces to a one-dimensional problem with absorbing boundary conditions at $r = \pm R$, with solution

$$\tau_{\rm MFP} = \frac{R^2}{2}\, {}_2F_2\left(1, 1; \frac{3}{2}, 2; \frac{R^2}{2}\right) \ , \tag{V.6}$$

for generalized hypergeometric function ${}_2F_2(a_1, a_2; b_1, b_2; z)$.

To compute the output power in (V.2), we need to determine the stead-state distribution for the trap-bead displacements L_n. Given an initial L_n, fixed ratchet time $\tau = \tau_{\rm MFP}$, and noise ξ_n, the trap-bead displacement after ratcheting is

$$L_{n+1} = \lambda^{(z)}_{n^+ + 1} - z_{n+1} \tag{V.7a}$$

$$= \sqrt{\left[(1 - {\rm e}^{-\tau})(L_n - \delta_{\rm g}) + \sqrt{1 - {\rm e}^{-2\tau}}\ \xi_n - L_n\right]^2 + R^2} \ . \tag{V.7b}$$

We obtain the propagator from L_n to L_{n+1} by integrating over all possible noise realizations, giving

$$T_L(L_{n+1}|L_n) \equiv \int_{-\infty}^{+\infty} {\rm d}\xi\ \delta\left(L_{n+1} - \sqrt{\left[(1 - {\rm e}^{-\tau})(L_n - \delta_{\rm g}) + \sqrt{1 - {\rm e}^{-2\tau}}\ \xi - L_n\right]^2 + R^2}\right) \mathcal{N}_1(\xi\,|\,0; 1) \tag{V.8a}$$

$$= \frac{L_{n+1}}{\sqrt{L_{n+1}^2 - R^2}} \left[\mathcal{N}_1\left(L_n - (1 - {\rm e}^{-\tau})(L_n - \delta_{\rm g}) \,\middle|\, \sqrt{L_{n+1}^2 - R^2}; \sigma(\tau)^2\right)\right.$$

$$\left. + \mathcal{N}_1\left(L_n - (1 - {\rm e}^{-\tau})(L_n - \delta_{\rm g}) \,\middle|\, -\sqrt{L_{n+1}^2 - R^2}; \sigma(\tau)^2\right)\right] \ . \tag{V.8b}$$

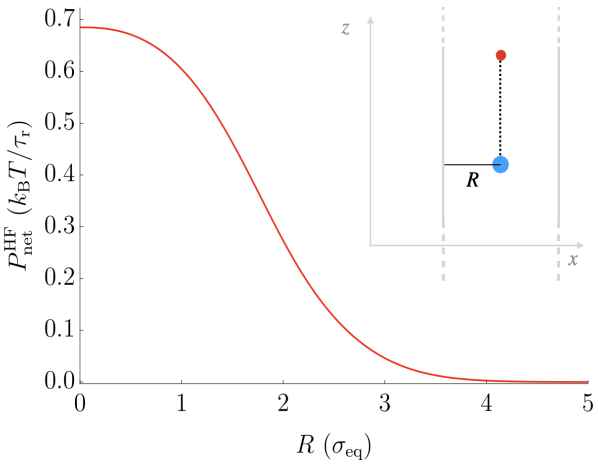

FIG. 2. Semi-analytic computation of output power $P_{\rm net}^{\rm HF}$ from Eq. (V.10) as a function of the threshold R in the transverse degree of freedom, for $d=2$ and $\delta_{\rm g}=0.8$. Inset: schematic showing bead (blue), trap center (red) and surrounding cylinder of radius R.

We obtain the steady-state distribution for the trap-bead displacement by solving the integral eigenvalue problem

$$\pi_L(L) = \int_0^\infty {\rm d}u\ T_L(L|u)\,\pi_L(u)\ . \tag{V.9}$$

Similar to SM IV, we solve the integral eigenvalue problem from Eq. (V.9) by discretizing the propagator $T_L(L|u)$ in a grid of $15,000 \times 15,000$ uniformly spaced points in the domain $L, u \in [0, 20]$. The corresponding steady-state solution is the leading eigenvector of $T_L(L|u)$, with eigenvalue 1. The recurrence-like structure of (V.7b) allows further simplification of the output power (V.2), giving

$$P_{\rm net}(R) = \frac{\delta_{\rm g}}{\tau}(1-{\rm e}^{-\tau})\left(\langle L\rangle - \delta_{\rm g}\right)\ . \tag{V.10}$$

Figure 2 shows the output power in the high-sampling-frequency limit as a function of R. The output power decreases monotonically with R, maximized at $R=0$. That is, for any positive threshold, the gain in extracted work per ratchet event is outweighed by the increased mean first-passage time between ratchet events.

VI. OUTPUT POWER FOR THE PARTIAL INFORMATION ENGINE

Here, for the partial information engine introduced in *Ignoring vertical fluctuations* in the main text, we derive the analytical expression for the output power $P_{\rm net}^{\rm HF}$ in Eq. (VI.11a). Since we do not know the steady-state distribution for the displacements $z_{n+1} - \lambda_{n^+}^{(z)}$ *a priori*, we consider the general family of feedback rules parametrized by ω,

$$\lambda_{n^+\!+1}^{(z)} = \lambda_{n^+}^{(z)} + \omega + \sqrt{\omega^2 + \sum_{j=1}^{d-1}\left(\Delta x_{n+1}^{(j)}\right)^2}\ , \tag{VI.1}$$

then compute the average $\left\langle z_{n+1} - \lambda_{n^+}^{(z)}\right\rangle$ and set ω to match the feedback rule (15). In this context, ω constitutes the (initially unknown) average change of the z-component of the trap-bead displacement. Here we derive a self-consistent equation for determining ω, in such a way that it matches the steady-state average value $\left\langle z_{n+1} - \lambda_{n^+}^{(z)}\right\rangle$.

First, we compute the average of the bead-trap displacements $z_n - \lambda_{n^+}^{(z)}$ after ratcheting:

$$\left\langle z_n - \lambda_{n^+}^{(z)}\right\rangle = \left\langle z_{n+1} - \lambda_{n^+\!+1}^{(z)}\right\rangle \tag{VI.2a}$$

$$= \left\langle z_{n+1} - \lambda_{n^+}^{(z)}\right\rangle - \omega - \mathcal{R}(\omega, t_{\rm s}) \tag{VI.2b}$$

$$= -\mathcal{R}(\omega, t_{\rm s})\ , \tag{VI.2c}$$

with

$$\mathcal{R}(\omega, t_\mathrm{s}) \equiv \left\langle \sqrt{\omega^2 + \sum_{j=1}^{d-1} \left(x_{n+1}^{(i)} - \lambda_{n^+}^{(i)} \right)^2} \right\rangle \tag{VI.3a}$$

$$= \frac{\Omega_d}{[2\pi\sigma(t_\mathrm{s})^2]^{d/2}} \int_0^\infty \mathrm{d}r \; r^{d-2} \sqrt{\omega^2 + r^2} \; \mathrm{e}^{-\frac{r^2}{2\sigma(t_\mathrm{s})^2}} \quad . \tag{VI.3b}$$

In Eq. (VI.3b), we have taken into account that, although we do not know the steady-state distribution for the relative displacement $z_{n+1} - \lambda_{n^+}^{(z)}$ before ratcheting, the transverse displacements $x_{n+1}^{(i)} - \lambda_{n^+}^{(i)}$, $i = 1, ..., d-1$, follow Gaussian distributions of zero mean and standard deviation $\sigma(t_\mathrm{s})$. We identify $\mathcal{R}(\omega, t_\mathrm{s})$ with the average radius of the hypersphere defined by the zero-work condition $\langle W_{n+1} \rangle = 0$ when z measurements are ignored—analogous to $|\boldsymbol{r}_{n+1} - \boldsymbol{\lambda}_{n^+}|$ from the feedback rule (10).

We compute the average from (VI.2a) using the Langevin equation (5) for z_{n+1}:

$$\left\langle z_n - \lambda_{n^+}^{(z)} \right\rangle = \left\langle z_{n+1} - \lambda_{n^+ + 1}^{(z)} \right\rangle \tag{VI.4a}$$

$$= \mathrm{e}^{-t_\mathrm{s}} \left\langle z_n - \lambda_{n^+}^{(z)} \right\rangle - (1 - \mathrm{e}^{-t_\mathrm{s}})\delta_\mathrm{g} - \omega - \mathcal{R}(\omega, t_\mathrm{s}) \tag{VI.4b}$$

$$= -\mathrm{e}^{-t_\mathrm{s}} \mathcal{R}(\omega, t_\mathrm{s}) - (1 - \mathrm{e}^{-t_\mathrm{s}})\delta_\mathrm{g} - \omega - \mathcal{R}(\omega, t_\mathrm{s}) \; . \tag{VI.4c}$$

Combining (VI.2a) and (VI.4a) gives a self-consistent equation for ω:

$$\omega = -\mathrm{e}^{-t_\mathrm{s}} \mathcal{R}(\omega, t_\mathrm{s}) - (1 - \mathrm{e}^{-t_\mathrm{s}})\delta_\mathrm{g} \; . \tag{VI.5}$$

We now compute the output power in the high-sampling-frequency limit. The average of the variation of the trap-center z-component over a short timestep $\mathrm{d}t$ is

$$\left\langle \mathrm{d}\lambda_{n^+ + 1}^{(z)} \right\rangle \equiv \left\langle \lambda_{n^+ + 1}^{(z)} - \lambda_{n^+}^{(z)} \right\rangle \tag{VI.6a}$$

$$= \left\langle \lambda_{n^+ + 1}^{(z)} - z_{n+1} \right\rangle + \left\langle z_{n+1} - \lambda_{n^+}^{(z)} \right\rangle \tag{VI.6b}$$

$$= \mathcal{R}(\omega, t_\mathrm{s}) + \omega \; . \tag{VI.6c}$$

Substituting the self-consistency equation (VI.5) for ω gives

$$\left\langle \mathrm{d}\lambda_{n^+ + 1}^{(z)} \right\rangle = \omega + \mathrm{e}^{t_\mathrm{s}} \left[-\omega - (1 - \mathrm{e}^{-t_\mathrm{s}})\delta_\mathrm{g} \right] \tag{VI.7a}$$

$$= -(\mathrm{e}^{t_\mathrm{s}} - 1)(\omega + \delta_\mathrm{g}) \tag{VI.7b}$$

$$\approx -t_\mathrm{s}(\omega + \delta_\mathrm{g}), \quad t_\mathrm{s} \ll 1 \; . \tag{VI.7c}$$

We also Taylor expand $\left\langle \mathrm{d}\lambda_{n^+ + 1}^{(z)} \right\rangle$ (from the definition of feedback rule (VI.1)) in t_s, given that for sufficiently short times, the displacements $\mathrm{d}x_{n+1}^{(i)}$ are also small, giving

$$\left\langle \mathrm{d}\lambda_{n^+ + 1}^{(z)} \right\rangle \approx \omega + |\omega| + \frac{1}{2|\omega|} \sum_{i=1}^{d-1} (\mathrm{d}x_{n+1}^{(i)})^2 \tag{VI.8a}$$

$$= -t_\mathrm{s} \frac{d-1}{\omega}, \quad t_\mathrm{s} \ll 1 \; . \tag{VI.8b}$$

Equation (VI.8a) is only consistent for $\omega < 0$, since $\left\langle \mathrm{d}\lambda_{n^+ + 1}^{(z)} \right\rangle$ must be an infinitesimal magnitude. From a physical standpoint, since the trap-bead displacement $\lambda_{n^+}^{(z)} - z_n$ before bead-position update is positive and the mean equilibrium bead position lies below the trap due to gravity, the average of $z_{n+1} - \lambda_{n^+}^{(z)}$ is consistently negative. Combining (VI.6a) and (VI.7a) gives a closed-form expression for ω in the high-sampling frequency limit,

$$\omega + \delta_\mathrm{g} - \frac{d-1}{\omega} = 0 \; , \tag{VI.9}$$

giving

$$\omega = -\frac{1}{2}\left[\delta_{\mathrm{g}} + \sqrt{\delta_{\mathrm{g}}^2 + 4(d-1)}\right] \ . \tag{VI.10}$$

Substituting Eq. (VI.10) into Eq. (VI.8) gives the output power

$$P_{\mathrm{net}}^{\mathrm{HF}} = \delta_{\mathrm{g}} \frac{\left\langle \mathrm{d}\lambda_{n^+ +1}^{(z)} \right\rangle}{t_{\mathrm{s}}} \tag{VI.11a}$$

$$\approx -\delta_{\mathrm{g}} \frac{d-1}{\omega} \tag{VI.11b}$$

$$= \frac{2(d-1)}{1 + \sqrt{1 + 4(d-1)/\delta_{\mathrm{g}}^2}} \ . \tag{VI.11c}$$

In the limit $\delta_{\mathrm{g}} \to \infty$, the output power simplifies to the asymptotic value $d-1$. Figure 4 shows Eq. (VI.11c) for the output power as a function of δ_{g}, for different dimensions d.

---

[1] T. K. Saha, J. N. E. Lucero, J. Ehrich, D. A. Sivak, and J. Bechhoefer, Maximizing power and velocity of an information engine, Proc. Natl. Acad. Sci. U.S.A. **118**, e2023356118 (2021).

[2] P. E. Kloeden and E. Platen, *Numerical Solution of Stochastic Differential Equations* (Springer Berlin Heidelberg, Berlin, Heidelberg, 1992).

[3] C. M. Bender and S. A. Orszag, *Advanced Mathematical Methods for Scientists and Engineers* (McGraw-Hill, 1978).